Atmos. Chem. Phys. Discuss., 13, 15907–15947, 2013
www.atmos-chem-phys-discuss.net/13/15907/2013/
doi:10.5194/acpd-13-15907-2013

Atmospheric Chemistry and Physics Discussions
Open Access

Analyzing experimental data and model parameters: implications for predictions of SOA using chemical transport models

K. C. Barsanti[1], **A. G. Carlton**[2], **and S. H. Chung**[3]

[1]Portland State University, Portland, Oregon, USA
[2]Rutgers University, New Brunswick, New Jersey, USA
[3]Washington State University, Pullman, Washington, USA

Received: 10 May 2013 – Accepted: 23 May 2013 – Published: 14 June 2013

Correspondence to: K. C. Barsanti (barsanti@pdx.edu)

Published by Copernicus Publications on behalf of the European Geosciences Union.

Abstract

Despite the critical importance for air quality and climate predictions, accurate representation of secondary organic aerosol (SOA) formation remains elusive. An essential addition to the ongoing discussion of improving model predictions is an acknowledgement of the linkages between experimental conditions, parameter optimization and model output, as well as the linkage between empirically-derived partitioning parameters and the physicochemical properties of SOA they represent in models. In this work, advantages of the volatility basis set (VBS) modeling approach are exploited to develop parameters for use in the computationally-efficient and widely-used two product (2p) SOA modeling framework, standard in chemical transport models such as CMAQ (Community Multiscale Air Quality) and GEOS-Chem (Goddard Earth Observing System–Chemistry). Calculated SOA yields and mass loadings obtained using the newly-developed 2p-VBS parameters and existing 2p and VBS parameters are compared with observed yields and mass loadings from a comprehensive list of published smog chamber studies to determine a "best available" set of SOA modeling parameters. SOA and $PM_{2.5}$ levels are simulated using CMAQv.4.7.1; results are compared for a base case (with default 2p CMAQ parameters) and two "best available" parameter cases chosen to illustrate the high- and low-NOx limits of biogenic SOA formation from monoterpenes. Comparisons of published smog chamber data with SOA yield predictions illustrate that: (1) SOA yields for naphthalene and cyclic and > C5 alkanes are not well represented using either newly developed (2p-VBS) or existing (2p and VBS) parameters for low-yield aromatics and lumped alkanes, respectively; and (2) for 4 of 7 volatile organic compound + oxidant systems, the 2p-VBS parameters better represent existing data. Using the "best available" parameters (combination of published 2p and newly derived 2p-VBS), predicted SOA mass and $PM_{2.5}$ concentrations increase by up to 10–15 % and 7 %, respectively, for the high-NOx case and up to 215 % ($\sim 3\,\mu g\,m^{-3}$) and 55 %, respectively, for the low-NOx case. The ability to robustly assign "best available" parameters, however, is limited due to insufficient data

ACPD
13, 15907–15947, 2013

for photo-oxidation of diverse monoterpenes and sesquiterpenes under a variety of atmospherically relevant NO_x conditions. These results are discussed in terms of implications for current chemical transport model simulations and recommendations are provided for future measurement and modeling efforts.

1 Introduction

Atmospheric fine particulate matter ($PM_{2.5}$) has long been linked to direct climate forcing, with estimates of radiative forcing due to the sulfate fraction surpassing that due to the organic carbon fraction (Haywood et al., 2000 and references therein). However, more recently, Goldstein et al. (2009) reported that for the southeastern United States (US) the spatial and temporal distributions of aerosol optical thickness (AOT) are most consistent with biogenic organic aerosol precursors (e.g., α-pinene), suggesting secondary organic aerosol (SOA) dominates AOT in the summer, thereby affecting negative radiative forcing or cooling in the region. A modeling study by Myhre et al. (2009) also suggests that SOA is a significant contributor to negative radiative forcing on a global scale; that contribution may increase dramatically (Park et al., 2010) if one considers the production of brown carbon by SOA constituents (Updyke et al., 2012). SOA, by virtue of its contribution to $PM_{2.5}$ (20–50 % globally, Hallquist et al., 2009), also plays a role in adversely affecting health (e.g., Pope et al., 2007). It is thus of critical importance that a quantitative and predictive understanding of SOA be achieved. To that end, much effort has been directed at developing, improving, and testing SOA models that are sufficiently comprehensive yet computationally efficient.

Accurate representation of SOA is elusive, even at the process-level, and becomes increasingly so as attempts are made to simplify and parameterize systems that are not fully understood. While the focus of this work is on bottom-up SOA modeling approaches, top-down approaches exist as well (e.g., Spracklen et al., 2011). One bottom-up approach to simulating SOA in three-dimensional chemical transport models (CTMs) proceeds by combining anthropogenic and biogenic emissions es-

ACPD
13, 15907–15947, 2013

timates with smog chamber data on SOA formation from individual volatile organic compound (VOC) precursors to generate regional and/or global SOA fields (Hallquist et al., 2009). SOA formation is based on gas/particle (G/P) partitioning theory (Pankow, 1994a,b) and historically parameterized using the two-product (2p) approach of Odum et al. (1996), in which up to two lumped products are assumed to represent the condensable oxidation products of each VOC + oxidant system. For each VOC + oxidant system, products are assigned empirically-derived partitioning parameters (K_p or C^*) and stoichiometric product yields (α) using a least-squares fitting approach, typically such that one product has a relatively lower α value and lower volatility (p1) and the other has a relatively higher α value and higher volatility (p2). An alternative, more recent approach is the volatility basis set (VBS) approach (Donahue et al., 2006; Lane et al., 2008b), in which C^* values are defined by fixed logarithmically-spaced bins (the volatility basis set) and least-squares fitting is used to assign α values (e.g., Pathak et al., 2007a). In addition to SOA formation from oxidation of volatile precursors ("traditional" SOA), the VBS approach has been used to parameterize SOA formation based on smog chamber studies of low to intermediate volatility precursors (Grieshop et al., 2009; Presto et al., 2010), including those precursors produced from the evaporation of primary organic aerosol (POA) (Grieshop et al., 2009). While there are a variety of limitations associated with using smog chamber data to derive model parameters to represent SOA formation in the real atmosphere (e.g., Kroll and Seinfeld, 2008), and more detailed modeling approaches are being developed (e.g., GECKO-A, Aumont et al., 2005; Lee-Taylor et al., 2011, and CNPG, Pankow and Barsanti, 2009; Barsanti et al., 2011), most widely-used approaches for predicting SOA in CTMs rely on parameterizations of chamber experiments. These CTMs include CAM-Chem (Lack et al., 2004; Heald et al., 2008), CMAQ (Carlton et al., 2010), GEOS-Chem (Henze and Seinfeld, 2006; Pye et al., 2010), GISS GCM (Chung and Seinfeld, 2002) and PMCAMx (Lane et al., 2008b; Tsimpidi et al., 2011).

Chamber studies conducted with very high initial precursor concentrations (and subsequently high reacted hydrocarbon levels, ΔHC), lead to very high organic aerosol

ACPD
13, 15907–15947, 2013

mass concentrations (M_o) relative to ambient conditions. Under such conditions, because higher M_o values favor SOA formation, even relatively volatile compounds contribute to SOA. In dark α-pinene ozonolysis experiments by Yu et al. (1999) essentially all of the SOA mass formed was attributed to identified oxidation products that are relatively volatile, with K_p values on the order of 10^{-6} to $10^{-1}\,m^3\,\mu g^{-1}$ ($C^* \approx 10^5$ to $10\,\mu g\,m^{-3}$). In more recent dark α-pinene ozonolysis experiments by Camredon et al. (2010), also at high M_o, all of the major monomeric oxidation products identified in the condensed phase had K_p values on the order of 10^{-5} to $10^{-1}\,m^3\mu g^{-1}$ ($C^* \approx 10^4$ to $10\,\mu g\,m^{-3}$). Only the products at the lowest end of these volatility distributions ($K_p = 10^{-1}\,m^3\,\mu g^{-1}$ or $C^* = 10\,\mu g\,m^{-3}$) would be expected to condense at an atmospherically relevant M_o of $\sim 5\,\mu g\,m^{-3}$, and for those products, only $\sim 50\,\%$ would be expected in the condensed phase (based on G/P partitioning theory, Pankow, 1994a).

With the 2p fitting approach, the relatively volatile products that are formed in significant quantities in experiments with high ΔHC levels (and thus high M_o) "mask" the presence of lower volatility products formed with much lower α values. Thus, lower volatility products may not be adequately represented by K_p values derived from high M_o chamber experiments, though such lower volatility products may explain all SOA formation in the atmosphere. Evidence for this has been provided by low M_o chamber experiments. For example Pathak et al. (2007a) observed, also for dark α-pinene ozonolysis experiments, that existing 2p parameters significantly underestimated SOA at low mass loadings (see also Presto and Donahue, 2006). The VBS fitting approach has some advantages over the 2p fitting approach that are achieved by fixing the volatility bins (C^* values) based on experimental and/or ambient M_o ranges and fitting only the α values. For a typical 4-species basis set (e.g., $C^* = \{0.1, 1, 10, 100\}\,\mu g\,m^{-3}$) the number of free parameters, four, is the same as with the 2p approach; however, the VBS parameters are much less covariant because the volatility space is fixed (Presto and Donahue, 2006). The VBS parameters also may be better able to represent SOA formation at low M_o, even when limited data exist.

ACPD
13, 15907–15947, 2013

While much of the above has been previously acknowledged, principles of G/P partitioning theory are used here to guide an analysis of the often overlooked, but non-trivial linkages between experimental conditions, parameter optimization, and predictions of SOA using CTMs. Furthermore, in an effort to take advantage of the robustness of the VBS fitting approach and the computational efficiency of the 2p modeling framework, parameters based on VBS fits (2p-VBS parameters) are introduced and evaluated. Analysis of predicted SOA yields and mass concentrations using the 2p, VBS, and 2p-VBS parameters are used to recommend the "best" parameters based on currently available data, to highlight current knowledge gaps, and to guide future chamber experiments and SOA modeling efforts.

2 Approach

2.1 Development of 2p-VBS parameters

In this section, the motivation and approach for developing the 2p-VBS parameters are described. Figure 1a and b illustrates the relationship between chamber M_o and ΔHC levels and predicted SOA yields and mass concentrations using 2p and VBS fitting approaches for dark α-pinene ozonolysis experiments (see Supplement Table S1 for a descriptive list of all experimental data). As introduced above, the fitted parameters are influenced both by the range in M_o, as well as the number of data points at low M_o levels. The 2p parameterization of Presto et al. (2005) did a reasonable job of representing observed yields for the experiments from which the parameterization was derived (Fig. 1a), but did not capture the observed SOA formation for the same VOC + oxidant system at ΔHC levels < 15 ppb (Fig. 1b). The data set from which the Presto et al. (2005) 2p parameters were derived notably had very few data points at low M_o, none at $M_o < 5\,\mu g\,m^{-3}$ and only two at $M_o < 10\,\mu g\,m^{-3}$. Results from Shilling et al. (2008) suggest that when sufficient data points were available at low M_o (Fig. 1a, b) both the 2p and VBS parameterizations represented the observed yields (Fig. 1a)

ACPD
13, 15907–15947, 2013

and captured the observed SOA formation at the lowest ΔHC levels (Fig. 1b). VBS parameters were derived here using the Presto et al. (2005) data set. Figure 1a, b illustrates that compared to the existing 2p parameterization (Presto et al., 2005), the VBS parameterization was better able to represent observed SOA formation at ΔHC levels < 15 ppb in the experiments from which the parameters were derived as well as in other chamber experiments for the same VOC + oxidant system (Griffin et al., 1999; Cocker et al., 2001a; Presto et al., 2005; Pathak et al., 2007b; Song et al., 2007). These results suggest that the VBS approach may be better able to represent SOA formation at low ΔHC levels and M_o, specifically when data are available but sparse.

In the context of chemical transport modeling, the inability of the Fig. 1 parameterizations to accurately capture SOA formation at low, atmospherically relevant ΔHC levels has important consequences for spatial and temporal predictions of atmospheric $PM_{2.5}$, as well as implications for analyses of the relative contribution of specific precursors to SOA, including source-attribution analyses. While the VBS approach may be better able to represent SOA formation at atmospherically relevant ΔHC levels and M_o, retaining source attribution in CTMs is computationally cost prohibitive for many applications. Therefore, in an effort to exploit the fitting advantages of the VBS approach and to retain the computationally-efficient, precursor-specific, and widely-used 2p modeling framework, 2p-VBS parameters were developed as follows. For the traditional SOA precursors, the VBS parameters of Tsimpidi et al. (2010) at $T = 298\,K$ were used to generate 263 pseudo-data points (yield vs. M_o) for $M_o = 0$ to $200\,\mu g\,m^{-3}$ at each of three temperatures (272, 298, and 324 K) using an effective $\Delta H_{vap} = 30\,kJ\,mol^{-1}$ (see Pathak et al., 2007b); those 789 pseudo-data points were then fit to generate a set of 2p-VBS parameters for each set of VBS parameters. The 2p-VBS parameters are reported in Table 1 for $T = 298\,K$ and $\rho = 1.5\,g\,cm^{-3}$ (the same temperature and assumed density reported in Tsimpidi et al. (2010); see Supplement for derivation of the density correction). In addition to the volatile SOA precursors, 2p-VBS parameters were derived for semi-volatile alkanes and POA (Table 2) based on the VBS parameters of Presto et al. (2010), Shrivastava et al. (2008) and Grieshop et al. (2009). Following

ACPD
13, 15907–15947, 2013

Shrivastava et al. (2008), the effective ΔH_{vap} was not fixed for POA (as was the case for the volatile SOA precursors, alkanes, and naphthalene) but was treated as an additional fitting parameter (included in Table 2). For each of the traditional SOA precursors, the 2p-VBS parameters reproduced the yield curves from the VBS parameters, at each of the three temperatures, and were able to represent SOA formation with the same degree of uncertainty as the VBS parameters (i.e., no additional error is introduced by the 2p-VBS fit, see Supplement Fig. S1). Thus it can be assumed that the SOA yield and mass predictions using the Tsimpidi et al. (2010) VBS parameters and the 2p-VBS parameters derived here produce equivalent results (in the absence of any "aging"), including the temperature dependence of SOA yields; therefore, only predictions using the 2p-VBS parameters are shown in subsequent figures (predictions from Tsimpidi et al. (2010) VBS parameters are not shown). It should be noted that the 2p-VBS parameters derived in this work are fundamentally different from the reduced (2-species) VBS parameters in Shrivastava et al. (2011), also developed to reduce computational burden, specifically in CTMs running online meteorology. Differences between the approaches and resulting parameters are described in the Supplement (see Fig. S2).

2.2 Chemical transport modeling

CMAQ (Byun and Schere, 2006) version 4.7.1 was used to simulate SOA mass concentrations over the continental US (12 × 12 km resolution) up to 50 mb with 34 vertical layers (4 666 194 grid cells) for 12–31 July 2006. This date range is representative of typical US summertime conditions when biogenic SOA is a measurable component of total $PM_{2.5}$ (Kleindienst et al., 2010). The simulation results for the first three days were excluded from the analysis to allow for model initialization and spin-up. The gas-phase chemistry mechanism SAPRC07 (Carter, 2010) was used for the simulations, with updated isoprene photo-oxidation chemistry to improve isoprene nitrate yields, isoprene nitrate lifetimes, and NO_x recycling rates (Xie et al., 2012). Anthropogenic emissions were based on the 2005 National Emissions Inventory (NEI) projected to 2006; biogenic emissions were generated with the Biogenic Emissions Inventory System (BEIS)

ACPD
13, 15907–15947, 2013

model version 3.14. Meteorological inputs for BEIS and pollutant transport were from version 3.1 of the Weather Research Forecasting (WRF) model. Three cases were considered: a base case using the revised CMAQv4.7 parameters (i.e., CMAQv4.7.1 parameters) described in Carlton et al. (2010) and two additional cases exploring "best available" SOA parameters and sensitivity to NO_x-dependent biogenic SOA formation (BA-highNOx and BA-lowNOx). Selection of the best available parameters was based on the comparison of 2p, VBS and 2p-VBS predictions with chamber data and is described in detail in the results and discussion section.

CMAQv4.7.1 allows NO_x-dependent SOA formation for anthropogenic precursors only (see Carlton et al., 2010); thus two case studies (BA-highNOx and BA-lowNOx) were constructed to illustrate the limits of SOA formation from monoterpenes under "high" and "low" NO_x conditions. For the aromatic precursors within CMAQ, the branching between the high- and low-NOx SOA formation pathways is treated dynamically as a function of the ratio of nitric oxide (NO) to hydroperoxy radical (HO_2) and the reaction rates of the peroxyradical (RO_2) with NO and HO_2 (Henze et al., 2008). Therefore, the anthropogenic high-NOx parameters were the same in the prescribed BA-highNOx and BA-lowNOx case studies, and were selected as described in the results and discussion section. For the anthropogenic low-NOx parameters, the default CMAQv4.7.1 values were used. While legitimate questions exist as to the relationship between NO_x conditions in chambers and NO_x conditions in the real atmosphere (and how each are defined), a detailed investigation is beyond the scope of this manuscript. For biogenic precursors, the division between high- and low-NOx experimental data and SOA parameterizations was thus based on a number of factors: (1) the designation given in the associated publications, (2) reported $HC_{initial}/NO_{x_{initial}}$ and/or $\Delta HC/NO_{x_{initial}}$ ratios, and (3) comparisons among reportedly similar data/parameterizations (see Supplement Table S1 for chamber experiment details). The selection of biogenic SOA parameters, specifically for monoterpenes, under high-NOx conditions (BA-highNOx) and low-NOx conditions (BA-lowNOx) is further described in the results and discussion section. The parameters selected for each case are summarized in Table 3.

ACPD
13, 15907–15947, 2013

3 Results and discussion

3.1 Biogenic precursor parameters

In Figs. 2–4, for each of the biogenic precursors (isoprene, monoterpenes, sesquiterpenes), two panels are shown. The first is SOA yield vs. M_o (panel a) and the second is M_o vs. ΔHC (panel b). Theoretical yield curves (panel a) and predicted SOA curves (panel b) using 2p, VBS, and/or 2p-VBS parameters are shown, along with chamber data. The predicted SOA curves are particularly well-suited for illustrating the ability (or inability) of model parameters to represent SOA formation under ambient conditions. Where sufficient chamber data were available, the figures were limited to $M_o < 10$–$30\,\mu g\,m^{-3}$ to further highlight the atmospherically relevant range. For the precursors that have been more widely studied (e.g., monoterpenes), a subset of published chamber data was selected based either on the use of the data in derivation of CTM model parameters or on the experimental conditions (relatively low/atmospherically relevant ΔHC levels and M_o). Parameters were evaluated for both high- and low-NOx conditions.

3.1.1 Isoprene parameters

In Fig. 2, the 2p-VBS theoretical yield (Fig. 2a) and SOA formation (Fig. 2b) curves for isoprene are compared with those from two additional parameterizations widely-used in chemical transport modeling: (1) the Henze and Seinfeld (2006) low-NOx 2p parameterization based on the chamber experiments of Kroll et al. (2006), and (2) the high-NOx "3p" parameterization of Pandis et al. (1991). Also shown are upper-bound (low-NOx) and lower-bound (high-NOx) parameterizations from Carlton et al. (2009) (note: the lower-bound parameterization is outside the axis range in Fig. 2b). For the low-NOx conditions, the 2p-VBS underpredicted SOA yields compared to chamber observations (Fig. 2a) and was not able to reproduce the observed SOA formation at the lowest ΔHC levels (Fig. 2b) (chamber data: Kroll et al., 2005, 2006; Chan et al., 2006;

ACPD
13, 15907–15947, 2013

Chhabra et al., 2010). The low-NOx 2p parameterizations of Henze and Seinfeld (2006) and of Carlton et al. (2009) were in better agreement with the observations (Kroll et al., 2006; Chhabra et al., 2010); both of which were derived directly from chamber data. In contrast, the low-NOx VBS parameterization was extrapolated from the high-NOx VBS parameterization as follows: the high-NOx VBS parameters (Lane et al., 2008a; Tsimpidi et al., 2010), based on the "3p" parameterization of Pandis et al. (1991), were adjusted using an M_o-dependent yield correction from the α-pinene experiments and parameterizations of Pathak et al. (2007a) as described in Lane et al. (2008a). It is thus not unexpected that the low-NOx 2p-VBS parameterization was not able to represent observed SOA formation, particularly at the lowest ΔHC levels. For the CMAQ simulations the default low-NOx parameters based on Henze and Seinfeld (2006), which notably produce the highest predicted SOA yields, are retained as the "best available".

There have been limited studies investigating the effects of NO_x on isoprene SOA yields (Carlton et al., 2009 and references therein). The parameterizations shown here suggest that increasing NO_x potentially results in lower SOA yields (Fig. 2a); however, as has been described by Surratt et al. (2010) and Chan et al. (2010), SOA yields are dependent on relative concentrations of HO_2, NO and NO_2, complicating the interpretation of NO_x dependence. For the high-NOx isoprene conditions, none of the parameterizations were able to represent the SOA yields (Fig. 2a) or SOA formation observed at the lowest, atmospherically relevant, ΔHC levels (Fig. 2b). Given that: (1) under some conditions, highest yields have been observed under high-NOx conditions when NO_2/NO ratios are high and $RO_2 + NO_2$ reactions are favored over $RO_2 + NO$ reactions (e.g., Chan et al., 2010); and (2) the effects of NOx on the volatility of the initially formed products (e.g., the point at which SOA formation is observed) are not clear (Fig. 2b), NO_x dependence of SOA formation by isoprene was not considered here. The default CMAQ low-NOx parameters (Henze and Seinfeld, 2006) were used in all simulations.

ACPD
13, 15907–15947, 2013

3.1.2 Monoterpene parameters

In Fig. 3, the 2p-VBS theoretical yield (Fig. 3a) and SOA formation (Fig. 3b) curves for lumped monoterpenes are compared with those obtained from parameterizations used in CMAQ v.4.7.1 (Carlton et al., 2010) and GEOS-Chem (Pye et al., 2010). Given the limited data available from photo-oxidation studies of monoterpenes, data are shown for dark α-pinene ozonolysis chamber experiments (low-NOx referenced in Fig. 1, high-NOx: Presto et al., 2005; Presto and Donahue, 2006; Ng et al., 2007a). As argued by Pye et al. (2010), the parameters derived from dark α-pinene ozonolysis experiments likely overestimate yields from photo-oxidation of α-pinene, but likely underestimate yields from photo-oxidation of other monoterpenes known to have higher yields than α-pinene, therefore potentially making dark α-pinene ozonolysis a good proxy for photo-oxidation of lumped monoterpenes.

The CMAQ (Carlton et al., 2010 high-NOx 2p parameters were based on the chamber experiments of Hoffmann et al. (1997) and Griffin et al. (1999); there is no low-NOx monoterpene SOA formation pathway in CMAQ v.4.7.1. In Pye et al. (2010), the low-NOx VBS parameters were based on dark α-pinene ozonolysis chamber experiments of Shilling et al. (2008). The low-NOx VBS parameters in Lane et al. (2008b)/Tsimpidi et al. (2010) were calculated as a weighted average for individual monoterpenes based on chamber studies under a range of experimental conditions (e.g., UV vs. dark, high vs. low RH). In Pye et al. (2010) and Lane et al. (2008a) the high-NOx VBS parameters were extrapolated from the low-NOx parameters as follows: (1) Pye et al. (2010) applied a fixed yield correction based on the α-pinene experiments of Ng et al. (2007a) and Pathak et al. (2007a), and (2) Lane et al. (2008a) applied a M_o-dependent yield correction based on Pathak et al. (2007a). The lower yields and mass concentrations predicted in this work with the 2p-VBS parameters, relative to those predicted with the Pye et al. (2010) VBS parameters, are a consequence of both the lower observed SOA yields for UV conditions (data used in low-NOx VBS parameterization) and the greater yield correction in calculating the high-NOx parameters. Note that while the use of the

ACPD
13, 15907–15947, 2013

high-NOx isoprene VBS parameters (Lane et al., 2008a) to obtain the low-NOx isoprene parameters leads to a likely underestimation of SOA formation (Fig. 2a), the use of the low-NOx monoterpene VBS parameters (Lane et al., 2008a; Pye et al., 2010) to obtain the high-NOx parameters leads to reasonable and perhaps an overestimation of SOA formation (Fig. 3). The high-NOx monoterpene parameterization of Pye et al. (2010), derived from the low-NOx Shilling et al. (2008) experiments, appears to overestimate SOA formation at low ΔHC and M_o levels (Fig. 3b). However, the data are insufficient to make robust conclusions, highlighting the need for monoterpene photo-oxidation studies under varying atmospherically relevant NO_x conditions. Based on the available data, the 2p-VBS parameters for both low- and high-NOx conditions were chosen for the CMAQ simulations.

3.1.3 Sesquiterpene parameters

In Fig. 4, the 2p-VBS theoretical yield (Fig. 4a) and predicted SOA (Fig. 4b) curves for lumped sesquiterpenes are compared with curves from the 2p parameterization used in CMAQ v.4.7.1 (Carlton et al., 2010) and the VBS parameterization in GEOS-Chem (Pye et al., 2010). Relative to the 2p and VBS parameterizations, the 2p-VBS parameterization underestimated SOA yields (Fig. 4a) and M_o (Fig. 4b) (chamber data: Griffin et al., 1999; Ng et al., 2007a). The VBS parameters (Lane et al., 2008b; Tsimpidi et al., 2010), on which the 2p-VBS parameters were based, and the CMAQ (Carlton et al., 2010) and Pye et al. (2010) parameters all were derived from chamber experiments involving α-humulene or β-caryophyllene as the sesquiterpene precursor; however, the Lane et al. (2008b)/Tsimpidi et al. (2010) VBS parameters were derived using data from photo-oxidation as well as dark ozonolysis experiments (Ng et al., 2006). For α-humulene or β-caryophyllene, the dark ozonolysis yields were significantly lower than the photo-oxidation yields, which likely resulted in the low bias of the Lane et al. (2008b) parameterization, and thus the low bias of the 2p-VBS parameterization as compared with CMAQ (Carlton et al., 2010) and GEOS-Chem (Pye et al., 2010).

ACPD
13, 15907–15947, 2013

Both the CMAQ (Carlton et al., 2010) and Pye et al. (2010) parameterizations were based on the chamber photo-oxidation data of Griffin et al. (1999), which had $\Delta HC[ppbC]/NO_{x_{initial}}[ppb]$ ratios of 0.5 to 8.0. The 2p parameterization of Carlton et al. (2010) was based on all 7 data points and was categorized as relevant for high-NOx conditions; whereas the VBS parameterization of Pye et al. (2010) was based on 4 of the 7 data points, with $\Delta HC[ppbC]/NO_{x_{initial}}[ppb] > 3$, and was categorized as relevant for low-NOx conditions. As shown in Fig. 4a, b the two parameterizations produced quantitatively similar results. These results are reflective of the Griffin et al. (1999) data from which no clear trend as a function of VOC/NO_x ratio was observed. The VOC/NO_x ratios span a much smaller range than that of Ng et al. (2007a), in which the high- and intermediate-NOx experiments all had $\Delta HC[ppbC]/NO_{x_{initial}}[ppb] \ll 1$ and the low-NOx experiments $\gg 50$; in addition, for all but one experiment ($\Delta HC[ppbC]/NO_{x_{initial}}[ppb] = 8$) the Griffin et al. (1999) conditions would be classified as high-NOx based on Presto et al. (2005). Somewhat surprisingly, the clear NO_x-dependency observed by Ng et al. (2007a) over all mass loadings ($M_o = 20–214\,\mu g\,m^{-3}$) is no longer observable at the lowest M_o (Fig. 4a, b). Instead there appears to be a greater dependence of SOA yields on the specific sesquiterpene precursor than on VOC/NO_x ratios (see Supplement Fig. S3).

Without the availability of additional data on the NO_x-dependency of SOA formation from different sesquiterpene precursors, the default CMAQv.4.7.1 parameters for sesquiterpenes were retained as the best available for high-NOx conditions and it was concluded that there were insufficient data to support the derivation and/or use of low-NOx sesquiterpene parameters. It is however noted that the CMAQ parameters are not physically realistic, as they indicate a relatively high increase in the mass of the condensing compounds relative to the precursor ($\alpha \approx 1.5$) without a substantial decrease in volatility (unless it is assumed that the sesquiterpene SOA is dominated by highly oxidized sesquiterpene fragments). This is a consequence of the system of least-squares fitting equations being underdetermined, and thus derived α and C^* values are non-unique. The single lumped sesquiterpene oxidation product is relatively

ACPD
13, 15907–15947, 2013

volatile ($C^* = 25\,\mu g\,m^{-3}$) compared to the lower volatility lumped product of isoprene ($C^* = 0.6\,\mu g\,m^{-3}$) and monoterpenes (2p-VBS, $C^* = 6\,\mu g\,m^{-3}$). Different combinations of derived α and C^* values would produce significantly different results when used in CTMs. In the case of sesquiterpenes, the published C^* value results in a calculated SOA yield of ~20 % at $M_o = 5\,\mu g\,m^{-3}$; this is in contrast to the reported SOA yields of 40–60 % (for M_o =10–20 $\mu g\,m^{-3}$) shown in Fig. 4. A test set of parameters, more in line with the monoterpene parameters, reproduced the observed chamber data reasonably well and resulted in a calculated SOA yield of ~45 % at $M_o = 5\,\mu g\,m^{-3}$. This finding supports the need for further constraints, additional chamber data, on sesquiterpene + oxidant systems.

3.2 Anthropogenic precursor parameters

In Figs. 5 and 6, theoretical yield curves (SOA yield vs. M_o) are shown for each of the anthropogenic precursors: lumped high-yield (refers to yield in the gas phase) aromatics (ARO1 in SAPRC, includes toluene), lumped low-yield aromatics (ARO2 in SAPRC, includes xylene), and lumped alkanes (ALK5 in SAPRC). The anthropogenic 2p, VBS, and 2p-VBS parameters were evaluated for high-NOx conditions only.

3.2.1 Toluene/ARO1 parameters

For toluene/ARO1, the calculated SOA yields were consistent with the data on which each of the parameterizations were based (Fig. 5a). Hildebrandt et al. (2009) reported a range of SOA yields that were highly sensitive to experimental conditions such as UV intensity, temperature, and NO_x levels. For comparable temperatures, the reported SOA yields of Hildebrandt et al. (2009) are higher than those of Ng et al. (2007b); the latter of which were used to derive the 2p parameters in CMAQ (Carlton et al., 2010). Hildebrandt et al. (2009) described the likely reasons for these discrepancies: temperature differences during the experiments (slightly higher in Ng et al. (2007b), less variable in Hildebrandt et al., 2009), differences in NO_2/NO ratios (NO_2 dominated

ACPD
13, 15907–15947, 2013

in Hildebrandt et al. (2009), a more atmospherically relevant mix in Ng et al., 2007b), and corrections for vapor losses to particles on walls in Hildebrandt et al. (2009). The Tsimpidi et al. (2010) parameters used to derive the 2p-VBS parameters were based on the data of Ng et al. (2007b) and Hildebrandt et al. (2009), and best represented the middle point of these two data sets (see Fig. 5a). The 2p-VBS parameters for toluene/ARO1 under high-NOx conditions were chosen for the CMAQ simulations.

3.2.2 Xylene/ARO2 parameters

The lumped aromatics category ARO2 in SAPRC07 (Carter, 2010) contains xylenes, as well as the PAH naphthalene. In Fig. 5b, chamber data using naphthalene precursors (Chan et al., 2009; Kautzman et al., 2010; Shakya and Griffin, 2010) was differentiated from chamber data using xylene (Cocker et al., 2001b; Song et al., 2005; Ng et al., 2007b; Zhou et al., 2011) and "other" ARO2 precursors, e.g., methyl- and ethylbenzenes (Odum et al., 1997). There were significant differences in yields among these ARO2 precursors, particularly between naphthalene and xylene/"other". These differences were reflected in the predicted SOA yields using the naphthalene VBS parameters of Pye et al. (2010), based on the chamber data of Chan et al. (2009), and the xylene 2p parameters of Carlton et al. (2010), based on the chamber data of Ng et al. (2007b). Each of these parameterizations represented the available data well, with the acknowledgement that neither parameterization was appropriate for naphthalene and xylenes/other lumped ARO2 compounds. The high-NOx naphthalene VBS parameters of Pye et al. (2010) were used to obtain 2p-VBS parameters, which are provided in Table 2. The naphthalene 2p-VBS parameters were not used in the CMAQ simulations because naphthalene is not treated explicitly in the SAPRC gas-phase chemical mechanism but is lumped with xylene.

The high-NOx ARO2 VBS parameters of Lane et al. (2008a); Tsimpidi et al. (2010), from which the 2p-VBS parameters were derived, were calculated from the low-NOx ARO2 VBS parameters (Lane et al., 2008b), based on the chamber data of Ng et al. (2007b), by applying a M_o-dependent yield correction based on the α-pinene

ACPD
13, 15907–15947, 2013

parameterizations of Pathak et al. (2007a). This approach led to a significant overestimation of SOA formation from xylene and other ARO2 aromatics (excluding naphthalene). Thus, the default CMAQ parameters for ARO2 under high-NOx conditions were retained as the best available.

3.2.3 Alkane/ALK5 parameters

The lumped alkane species ALK5 includes C6 and higher cycloalkanes, C7 and higher *n*-alkanes, and C8 and higher branched alkanes. From an emissions perspective, the lumped ALK5 species is largely representative of a ∼ C8 alkane (e.g., Carlton et al., 2010; Pye and Pouliot, 2012). The CMAQ ALK5 parameters are from Pandis et al. (1992)/Strader et al. (1999), based on the chamber experiments of Grosjean and Seinfeld (1989); they roughly represent SOA formation from C8-C10 *n*-alkanes as measured by Grosjean and Seinfeld (1989). The VBS parameters (Lane et al., 2008b; Tsimpidi et al., 2010) used to obtain the 2p-VBS parameters were based on chamber data of Wang et al. (1992), Takekawa et al. (2003), and Lim and Ziemann (2005) for C8-C15 *n*-alkanes and methylcylcohexane (Wang et al., 1992). Due to limited data availability, both Pandis et al. (1992) and Lane et al. (2008b) derived only one-product fits for this class of lumped alkanes. Calculated SOA yields with the CMAQ 2p parameters (Carlton et al., 2010) and 2p-VBS parameters were compared with chamber data from Lim and Ziemann (2009) for linear and cyclic C8 alkanes (Fig. 6). The default CMAQ parameters were in good agreement with the Lim and Ziemann data for linear C8 alkanes (Fig. 6a), though may overestimate SOA at lower M_o (Fig. 6b). The 2p-VBS parameters resulted in higher SOA yields at higher ΔHC and M_o levels. This was likely due to the inclusion of cyclic alkane data in the fitting. Lim and Ziemann (2009) demonstrated that alkane SOA yields followed the trend: cyclic alkanes > linear alkanes > branched alkanes; in addition within each class, SOA yields increased with carbon number.

In addition to 2p and 2p-VBS parameters, VBS parameters from Presto et al. (2010) were compared with the data of Lim and Ziemann (2009) (Fig. 6). Presto et al. (2010)

ACPD
13, 15907–15947, 2013

derived VBS parameters for C12-C17 *n*-alkanes, based on *n*-heptadecane data (2p-VBS parameters based on Presto et al. (2010) are provided in Table 2). The theoretical yield curves and data points showed an increase in SOA yield as a function of carbon number, as observed by Lim and Ziemann (2009). At high M_o, the calculated SOA yields were higher than the reported yields of Lim and Ziemann (2009), particularly for the C12 alkanes (Fig. 6a); however, the experiments were conducted over very different M_o ranges with no overlapping data points and thus, the yields may not be directly comparable. At low M_o, there are no data points for evaluation, other than those from which the parameterization of Presto et al. (2010) was derived (Fig. 6b). Based on current emissions inventories and the parameterizations of Presto et al. (2010), the 2p-VBS parameters were chosen the best available.

The SOA yields from cyclic and C12 and higher *n*-alkanes (Fig. 6) and naphthalene (Fig. 5) were significantly underestimated by the default 2p parameters for the volatile SOA precursors with which they are lumped (cyclic and > C12 alkanes with ALK5 and naphthalene with ARO2) in the gas-phase chemical mechanism SAPRC07 (Carter, 2010). If emissions of such compounds are indeed sufficient to contribute measurably to SOA, as indicated by ambient observations (alkanes: Liu et al., 2011; Russell et al., 2011; de Gouw et al., 2011; naphthalene: Chan et al., 2009; Shakya and Griffin, 2010; Zhang and Ying, 2012), separation in the gas-phase and aerosol models likely will result in more accurate SOA predictions. Pye and Pouliot (2012) recently reported on the explicit treatment of C6-C19 alkanes and PAHs, represented by naphthalene, in CMAQv.5.0. They concluded that C6-C19 alkanes and PAHs could represent 20–30 % of SOA formation with highest contributions in winter, using current emissions inventories. Though similar modification of SAPRC07 and CMAQv4.7.1 is outside the scope of this study, it is recommended that SOA formation by cyclic alkanes, ≥ C12 *n*-alkanes and naphthalene be treated independently in future model applications.

ACPD
13, 15907–15947, 2013

3.3 CMAQ model simulations

The base case CMAQ predictions for total SOA, averaged over 15–31 July 2006 are shown in Fig. 7. In regions with the highest predicted concentrations of anthropogenic SOA ($< 1\,\mu g\,m^{-3}$), a net decrease in anthropogenic SOA (up to 20 %) was predicted (figure not shown); the use of best available parameters for ARO1/toluene (2p-VBS) resulted in a slight increase in predicted SOA mass while the use of best available parameters for ALK5 (2p-VBS) resulted in a slight decrease. In regions with the highest predicted concentrations of biogenic SOA ($1–2\,\mu g\,m^{-3}$ in northern California, southern Oregon and southeastern US), the predicted increase in total SOA mass was significant, ∼ 10–15 % for high-NOx conditions and up to ∼ 215 % ($\sim 3\,\mu g\,m^{-3}$) for low-NOx conditions (see Fig. 8). The increase in total SOA was largely driven by an increase in biogenic SOA (see Supplement Fig. S4) and the use of the 2p-VBS parameters for lumped monoterpenes. The predicted increases in total SOA correspond to increases in $PM_{2.5}$ of up to 7 % and 55 % for the high- and low-NOx conditions, respectively, in western US where $PM_{2.5}$ concentrations in the base case were on the order of $2\,\mu g\,m^{-3}$. The 2p-VBS fitting resulted in a 2-fold decrease in the C_1^* value for lumped monoterpenes (high-NOx), from $C_1^* = 14.8\,\mu g\,m^{-3}$ (default) to $C_1^* = 6.3\,\mu g\,m^{-3}$, which increased the predicted contribution of traditional monoterpene SOA (excluding oligomerization) to total SOA by ∼ 10 % in the southeastern US (from 15–30 % in base case, figure not shown). Under low-NOx conditions, that contribution is increased by ∼ 20–30 % in the southeastern US (figure not shown).

Figure 9 shows the fraction of RO_2 reacting with NO as compared to that reacting with HO_2, and thus the fractional weighting of high- vs. low-NOx parameters, illustrating the relative importance of high- vs. low-NOx pathways in the CMAQ simulations. As noted previously, this fractional weighting is considered in CMAQv.4.7.1 for anthropogenic precursors only, therefore the sensitivity simulations performed here using the high- and low-NOx 2p-VBS monoterpene parameters indicate the range of SOA that can be formed for the limiting assumptions. It can be seen in Fig. 9 that based on cur-

ACPD
13, 15907–15947, 2013

rent treatment, low-NOx pathways and therefore low-NOx parameters, are relevant for SOA formation in many regions of the US.

4 Conclusions

The linkages between experimental conditions, parameter optimization, and predictions of SOA were explored here by: (1) comparing calculated SOA yields and mass concentrations using 2p, VBS, and newly-developed 2p-VBS parameters with published chamber data for common precursor species; (2) selecting a set of "best available" (BA) parameters; and (3) analyzing CMAQv4.7.1 model output for the default (base case) and selected sensitivity (BA-highNOx and BA-lowNOx) simulations. With regard to parameter fitting, VBS parameterizations may be more robust when data are sparse; however, this alone is not sufficient to overcome the limited availability of chamber data, particularly for certain precursors, at low, atmospherically relevant ΔHC and M_0. Extrapolating from high- to low-NOx conditions, and vice versa, does not appear to produce reliable parameters, particularly when extrapolating from one precursor to another; data are required for each precursor under a range of NOx levels (NO_2/NO ratios). For the common SOA precursors treated in the 2p framework, data gaps are most significant for photo-oxidation of monoterpenes and sesquiterpenes under a range of $HO_2 : NO : NO_2$levels.

While only SOA formation in the traditional view was considered, VOC oxidation followed by condensation of semi-volatile oxidation products, some insight was gained on intermediate-volatility organic compound (IVOC) SOA precursors. The SOA yields from naphthalene and C12 and higher *n*-alkanes, which are currently lumped with VOCs in the gas-phase chemical mechanism SAPRC07 (Carter, 2010), were significantly underestimated by the default 2p parameters. 2p-VBS parameters are provided for these IVOC precursors, as well as POA, though the current SAPRC07/CMAQv4.7.1 configuration did not allow for their evaluation in the context of chemical transport modeling.

ACPD
13, 15907–15947, 2013

Recognizing the importance of processes not currently treated in the CMAQ SOA model (e.g., gas-phase aging beyond that typically captured in chamber studies and partitioning of POA), CTM predictions were not compared with ambient measurements. Nonetheless, the choice of model parameters will impact source-attribution analyses, as demonstrated, as well as spatial and temporal distributions of modeled SOA (through the physicochemical properties of SOA they represent), which may adversely affect the accuracy of air quality and climate predictions from CTMs that rely on rely on parameterizations of chamber experiments.

Supplementary material related to this article is available online at: http://www.atmos-chem-phys-discuss.net/13/15907/2013/acpd-13-15907-2013-supplement.pdf.

References

Aumont, B., Szopa, S., and Madronich, S.: Modelling the evolution of organic carbon during its gas-phase tropospheric oxidation: development of an explicit model based on a self generating approach, Atmos. Chem. Phys., 5, 2497–2517, doi:10.5194/acp-5-2497-2005, 2005.

Barsanti, K. C., Smith, J. N., and Pankow, J. F.: Application of the np plus mP modeling approach for simulating secondary organic particulate matter formation from alpha-pinene oxidation, Atmos. Environ., 45, 6812–6819, doi:10.1016/j.atmosenv.2011.01.038, 2011.

Byun, D. and Schere, K. L.: Review of the governing equations, computational algorithms, and other components of the models-3 Community Multiscale Air Quality (CMAQ) modeling system, Appl. Mech. Rev., 59, 51–77, doi:10.1115/1.2128636, 2006.

Camredon, M., Hamilton, J. F., Alam, M. S., Wyche, K. P., Carr, T., White, I. R., Monks, P. S., Rickard, A. R., and Bloss, W. J.: Distribution of gaseous and particulate organic composition during dark α-pinene ozonolysis, Atmos. Chem. Phys., 10, 2893–2917, doi:10.5194/acp-10-2893-2010, 2010.

Carlton, A. G., Wiedinmyer, C., and Kroll, J. H.: A review of Secondary Organic Aerosol (SOA) formation from isoprene, Atmos. Chem. Phys., 9, 4987–5005, doi:10.5194/acp-9-4987-2009, 2009.

ACPD
13, 15907–15947, 2013

Carlton, A. G., Bhave, P. V., Napelenok, S. L., Edney, E. D., Sarwar, G., Pinder, R. W., Pouliot, G. A., and Houyoux, M.: Model Representation of Secondary Organic Aerosol in CMAQv4.7, Environ. Sci. Technol., 44, 8553–8560, doi:10.1021/es100636q, 2010.

Carter, W. P. L.: Development of the SAPRC-07 chemical mechanism, Atmos. Environ., 44, 5324–5335, doi:10.1016/j.atmosenv.2010.01.026, 2010.

Chan, A. W. H., Kautzman, K. E., Chhabra, P. S., Surratt, J. D., Chan, M. N., Crounse, J. D., Kürten, A., Wennberg, P. O., Flagan, R. C., and Seinfeld, J. H.: Secondary organic aerosol formation from photooxidation of naphthalene and alkylnaphthalenes: implications for oxidation of intermediate volatility organic compounds (IVOCs), Atmos. Chem. Phys., 9, 3049–3060, doi:10.5194/acp-9-3049-2009, 2009.

Chan, A. W. H., Chan, M. N., Surratt, J. D., Chhabra, P. S., Loza, C. L., Crounse, J. D., Yee, L. D., Flagan, R. C., Wennberg, P. O., and Seinfeld, J. H.: Role of aldehyde chemistry and NO_x concentrations in secondary organic aerosol formation, Atmos. Chem. Phys., 10, 7169–7188, doi:10.5194/acp-10-7169-2010, 2010.

Chhabra, P. S., Flagan, R. C., and Seinfeld, J. H.: Elemental analysis of chamber organic aerosol using an aerodyne high-resolution aerosol mass spectrometer, Atmos. Chem. Phys., 10, 4111–4131, doi:10.5194/acp-10-4111-2010, 2010.

Chung, S. H. and Seinfeld, J. H.: Global distribution and climate forcing of carbonaceous aerosols, J. Geophys. Res.-Atmos., 107, 4407, doi:10.1029/2001jd001397, 2002.

Cocker, D. R., Clegg, S. L., Flagan, R. C., and Seinfeld, J. H.: The effect of water on gas-particle partitioning of secondary organic aerosol, Part I: alpha-pinene/ozone system, Atmos. Environ., 35, 6049–6072, doi:10.1016/s1352-2310(01)00404-6, 2001a.

Cocker, D. R., Mader, B. T., Kalberer, M., Flagan, R. C., and Seinfeld, J. H.: The effect of water on gas-particle partitioning of secondary organic aerosol: II. m-xylene and 1,3,5-trimethylbenzene photooxidation systems, Atmos. Environ., 35, 6073–6085, doi:10.1016/s1352-2310(01)00405-8, 2001b.

de Gouw, J. A., Middlebrook, A. M., Warneke, C., Ahmadov, R., Atlas, E. L., Bahreini, R., Blake, D. R., Brock, C. A., Brioude, J., Fahey, D. W., Fehsenfeld, F. C., Holloway, J. S., Le Henaff, M., Lueb, R. A., McKeen, S. A., Meagher, J. F., Murphy, D. M., Paris, C., Parrish, D. D., Perring, A. E., Pollack, I. B., Ravishankara, A. R., Robinson, A. L., Ryerson, T. B., Schwarz, J. P., Spackman, J. R., Srinivasan, A., and Watts, L. A.: Organic aerosol formation downwind from the deepwater horizon oil spill, Science, 331, 1295–1299, doi:10.1126/science.1200320, 2011.

ACPD
13, 15907–15947, 2013

Donahue, N. M., Robinson, A. L., Stanier, C. O., and Pandis, S. N.: Coupled partitioning, dilution, and chemical aging of semivolatile organics, Environ. Sci. Technol., 40, 2635–2643, doi:10.1021/es052297c, 2006.

Goldstein, A. H., Koven, C. D., Heald, C. L., and Fung, I. Y.: Biogenic carbon and anthropogenic pollutants combine to form a cooling haze over the southeastern United States, P. Natl. Acad. Sci. USA, 106, 8835–8840, doi:10.1073/pnas.0904128106, 2009.

Grieshop, A. P., Miracolo, M. A., Donahue, N. M., and Robinson, A. L.: Constraining the volatility distribution and gas-particle partitioning of combustion aerosols using isothermal dilution and thermodenuder measurements, Environ. Sci. Technol., 43, 4750–4756, doi:10.1021/es8032378, 2009.

Griffin, R. J., Cocker, D. R., Flagan, R. C., and Seinfeld, J. H.: Organic aerosol formation from the oxidation of biogenic hydrocarbons, J. Geophys. Res.-Atmos., 104, 3555–3567, 1999.

Grosjean, D. and Seinfeld, J. H.: Parameterization of the formation potential of secondary organic aerosolsq, Atmos. Environ., 23, 1733–1747, doi:10.1016/0004-6981(89)90058-9, 1989.

Hallquist, M., Wenger, J. C., Baltensperger, U., Rudich, Y., Simpson, D., Claeys, M., Dommen, J., Donahue, N. M., George, C., Goldstein, A. H., Hamilton, J. F., Herrmann, H., Hoffmann, T., Iinuma, Y., Jang, M., Jenkin, M. E., Jimenez, J. L., Kiendler-Scharr, A., Maenhaut, W., McFiggans, G., Mentel, Th. F., Monod, A., Prévôt, A. S. H., Seinfeld, J. H., Surratt, J. D., Szmigielski, R., and Wildt, J.: The formation, properties and impact of secondary organic aerosol: current and emerging issues, Atmos. Chem. Phys., 9, 5155–5236, doi:10.5194/acp-9-5155-2009, 2009.

Haywood, J. and Boucher, O.: Estimates of the direct and indirect radiative forcing due to tropospheric aerosols: a review, Rev. Geophys., 38, 513–543, 2000.

Heald, C. L., Henze, D. K., Horowitz, L. W., Feddema, J., Lamarque, J. F., Guenther, A., Hess, P. G., Vitt, F., Seinfeld, J. H., Goldstein, A. H., and Fung, I.: Predicted change in global secondary organic aerosol concentrations in response to future climate, emissions, and land use change, J. Geophys. Res.-Atmos., 113, D05211, doi:10.1029/2007jd009092, 2008.

Henze, D. K. and Seinfeld, J. H.: Global secondary organic aerosol from isoprene oxidation, Geophys. Res. Lett., 33, L09812, doi:10.1029/2006gl025976, 2006.

Henze, D. K., Seinfeld, J. H., Ng, N. L., Kroll, J. H., Fu, T.-M., Jacob, D. J., and Heald, C. L.: Global modeling of secondary organic aerosol formation from aromatic hydrocarbons: high-

ACPD
13, 15907–15947, 2013

vs. low-yield pathways, Atmos. Chem. Phys., 8, 2405–2420, doi:10.5194/acp-8-2405-2008, 2008.
Hildebrandt, L., Donahue, N. M., and Pandis, S. N.: High formation of secondary organic aerosol from the photo-oxidation of toluene, Atmos. Chem. Phys., 9, 2973–2986, doi:10.5194/acp-9-2973-2009, 2009.
Hoffmann, T., Odum, J. R., Bowman, F., Collins, D., Klockow, D., Flagan, R. C., and Seinfeld, J. H.: Formation of organic aerosols from the oxidation of biogenic hydrocarbons, J. Atmos. Chem., 26, 189–222, 1997.
Kautzman, K. E., Surratt, J. D., Chan, M. N., Chan, A. W. H., Hersey, S. P., Chhabra, P. S., Dalleska, N. F., Wennberg, P. O., Flagan, R. C., and Seinfeld, J. H.: Chemical composition of gas- and aerosol-phase products from the photooxidation of naphthalene, J. Phys. Chem. A, 114, 913–934, doi:10.1021/jp908530s, 2010.
Kleindienst, T. E., Lewandowski, M., Offenberg, J. H., Edney, E. O., Jaoui, M., Zheng, M., Ding, X. A., and Edgerton, E. S.: Contribution of primary and secondary sources to organic aerosol and $PM_{2.5}$ at SEARCH network sites, J. Air Waste Manage., 60, 1388–1399, doi:10.3155/1047-3289.60.11.1388, 2010.
Kroll, J. H. and Seinfeld, J. H.: Chemistry of secondary organic aerosol: formation and evolution of low-volatility organics in the atmosphere, Atmos. Environ., 42, 3593–3624, doi:10.1016/j.atmosenv.2008.01.003, 2008.
Kroll, J. H., Ng, N. L., Murphy, S. M., Flagan, R. C., and Seinfeld, J. H.: Secondary organic aerosol formation from isoprene photooxidation under high-NO(x) conditions, Geophys. Res. Lett., 32, L18808, doi:10.1029/2005gl023637, 2005.
Kroll, J. H., Ng, N. L., Murphy, S. M., Flagan, R. C., and Seinfeld, J. H.: Secondary organic aerosol formation from isoprene photooxidation, Environ. Sci. Technol., 40, 1869–1877, doi:10.1021/es0524301, 2006.
Lack, D. A., Tie, X. X., Bofinger, N. D., Wiegand, A. N., and Madronich, S.: Seasonal variability of secondary organic aerosol: a global modeling study, J. Geophys. Res.-Atmos., 109, D03203, doi:10.1029/2003jd003418, 2004.
Lane, T. E., Donahue, N. M., and Pandis, S. N.: Effect of NO(x) on secondary organic aerosol concentrations, Environ. Sci. Technol., 42, 6022–6027, doi:10.1021/es703225a, 2008a.
Lane, T. E., Donahue, N. M., and Pandis, S. N.: Simulating secondary organic aerosol formation using the volatility basis-set approach in a chemical transport model, Atmos. Environ., 42, 7439–7451, doi:10.1016/j.atmosenv.2008.06.026, 2008b.

ACPD
13, 15907–15947, 2013

Lee-Taylor, J., Madronich, S., Aumont, B., Baker, A., Camredon, M., Hodzic, A., Tyndall, G. S., Apel, E., and Zaveri, R. A.: Explicit modeling of organic chemistry and secondary organic aerosol partitioning for Mexico City and its outflow plume, Atmos. Chem. Phys., 11, 13219–13241, doi:10.5194/acp-11-13219-2011, 2011.

Lim, Y. B. and Ziemann, P. J.: Products and mechanism of secondary organic aerosol formation from reactions of *n*-alkanes with OH radicals in the presence of NO_x, Environ. Sci. Technol., 39, 9229–9236, doi:10.1021/es051447g, 2005.

Lim, Y. B. and Ziemann, P. J.: Effects of molecular structure on aerosol yields from oh radical–initiated reactions of linear, branched, and cyclic alkanes in the presence of NO_x, Environ. Sci. Technol., 43, 2328–2334, doi:10.1021/es803389s, 2009.

Liu, S., Day, D. A., Shields, J. E., and Russell, L. M.: Ozone-driven daytime formation of secondary organic aerosol containing carboxylic acid groups and alkane groups, Atmos. Chem. Phys., 11, 8321–8341, doi:10.5194/acp-11-8321-2011, 2011.

Myhre, G., Berglen, T. F., Johnsrud, M., Hoyle, C. R., Berntsen, T. K., Christopher, S. A., Fahey, D. W., Isaksen, I. S. A., Jones, T. A., Kahn, R. A., Loeb, N., Quinn, P., Remer, L., Schwarz, J. P., and Yttri, K. E.: Modelled radiative forcing of the direct aerosol effect with multi-observation evaluation, Atmos. Chem. Phys., 9, 1365–1392, doi:10.5194/acp-9-1365-2009, 2009.

Ng, N. L., Kroll, J. H., Keywood, M. D., Bahreini, R., Varutbangkul, V., Flagan, R. C., Seinfeld, J. H., Lee, A., and Goldstein, A. H.: Contribution of first- versus second-generation products to secondary organic aerosols formed in the oxidation of biogenic hydrocarbons, Environ. Sci. Technol., 40, 2283–2297, doi:10.1021/es052269u, 2006.

Ng, N. L., Chhabra, P. S., Chan, A. W. H., Surratt, J. D., Kroll, J. H., Kwan, A. J., McCabe, D. C., Wennberg, P. O., Sorooshian, A., Murphy, S. M., Dalleska, N. F., Flagan, R. C., and Seinfeld, J. H.: Effect of NO_x level on secondary organic aerosol (SOA) formation from the photooxidation of terpenes, Atmos. Chem. Phys., 7, 5159–5174, doi:10.5194/acp-7-5159-2007, 2007a.

Ng, N. L., Kroll, J. H., Chan, A. W. H., Chhabra, P. S., Flagan, R. C., and Seinfeld, J. H.: Secondary organic aerosol formation from *m*-xylene, toluene, and benzene, Atmos. Chem. Phys., 7, 3909–3922, doi:10.5194/acp-7-3909-2007, 2007b.

Odum, J. R., Hoffmann, T., Bowman, F., Collins, D., Flagan, R. C., and Seinfeld, J. H.: Gas/particle partitioning and secondary organic aerosol yields, Environ. Sci. Technol., 30, 2580–2585, 1996.

ACPD
13, 15907–15947, 2013

Odum, J. R., Jungkamp, T. P. W., Griffin, R. J., Forstner, H. J. L., Flagan, R. C., and Seinfeld, J. H.: Aromatics, reformulated gasoline, and atmospheric organic aerosol formation, Environ. Sci. Technol., 31, 1890–1897, doi:10.1021/es960535l, 1997.

Pandis, S. N., Paulson, S. E., Seinfeld, J. H., and Flagan, R. C.: Aerosol formation in the photooxidation of isoprene and beta-pinene, Atmos. Environ. Part a-General Topics, 25, 997–1008, doi:10.1016/0960-1686(91)90141-s, 1991.

Pandis, S. N., Harley, R. A., Cass, G. R., and Seinfeld, J. H.: Secondary organic aerosol formation and transport, Atmos. Environ. A, 26, 2269–2282, doi:10.1016/0960-1686(92)90358-r, 1992.

Pankow, J. F.: An absorption-model of gas-particle partitioning of organic-compounds in the atmosphere, Atmos. Environ., 28, 185–188, 1994a.

Pankow, J. F.: An absorption-model of the gas aerosol partitioning involved in the formation of secondary organic aerosol, Atmos. Environ., 28, 189–193, 1994b.

Pankow, J. F. and Barsanti, K. C.: The carbon number-polarity grid: A means to manage the complexity of the mix of organic compounds when modeling atmospheric organic particulate matter, Atmos. Environ., 43, 2829–2835, doi:10.1016/j.atmosenv.2008.12.050, 2009.

Park, R. J., Kim, M. J., Jeong, J. I., Youn, D., and Kim, S.: A contribution of brown carbon aerosol to the aerosol light absorption and its radiative forcing in East Asia, Atmos. Environ., 44, 1414–1421, doi:10.1016/j.atmosenv.2010.01.042, 2010.

Pathak, R. K., Presto, A. A., Lane, T. E., Stanier, C. O., Donahue, N. M., and Pandis, S. N.: Ozonolysis of α-pinene: parameterization of secondary organic aerosol mass fraction, Atmos. Chem. Phys., 7, 3811–3821, doi:10.5194/acp-7-3811-2007, 2007a.

Pathak, R. K., Stanier, C. O., Donahue, N. M., and Pandis, S. N.: Ozonolysis of alpha-pinene at atmospherically relevant concentrations: temperature dependence of aerosol mass fractions (yields), J. Geophys. Res.-Atmos., 112, D03201, doi:10.1029/2006jd007436, 2007b.

Pope, C. A.: Mortality effects of longer term exposures to fine particulate air pollution: review of recent epidemiological evidence, Inhalat. Toxicol., 19, 33–38, doi:10.1080/08958370701492961, 2007.

Presto, A. A. and Donahue, N. M.: Investigation of alpha-pinene plus ozone secondary organic aerosol formation at low total aerosol mass, Environ. Sci. Technol., 40, 3536–3543, doi:10.1021/es052203z, 2006.

ACPD
13, 15907–15947, 2013

Presto, A. A., Hartz, K. E. H., and Donahue, N. M.: Secondary organic aerosol production from terpene ozonolysis, 1. Effect of UV radiation, Environ. Sci. Technol., 39, 7036–7045, doi:10.1021/es050174m, 2005.

Presto, A. A., Miracolo, M. A., Donahue, N. M., and Robinson, A. L.: Secondary organic aerosol formation from high-NOx photo-oxidation of low volatility precursors: *n*-alkanes, Environ. Sci. Technol., 44, 2029–2034, doi:10.1021/es903712r, 2010.

Pye, H. O. T. and Pouliot, G. A.: Modeling the role of alkanes, polycyclic aromatic hydrocarbons, and their oligomers in secondary organic aerosol formation, Environ. Sci. Technol., 46, 6041–6047, doi:10.1021/es300409w, 2012.

Pye, H. O. T., Chan, A. W. H., Barkley, M. P., and Seinfeld, J. H.: Global modeling of organic aerosol: the importance of reactive nitrogen (NO_x and NO_3), Atmos. Chem. Phys., 10, 11261–11276, doi:10.5194/acp-10-11261-2010, 2010.

Russell, L. M., Bahadur, R., and Ziemann, P. J.: Identifying organic aerosol sources by comparing functional group composition in chamber and atmospheric particles, P. Natl. Acad. Sci. USA, 108, 3516–3521, doi:10.1073/pnas.1006461108, 2011.

Shakya, K. M. and Griffin, R. J.: Secondary organic aerosol from photooxidation of polycyclic aromatic hydrocarbons, Environ. Sci. Technol., 44, 8134–8139, doi:10.1021/es1019417, 2010.

Shilling, J. E., Chen, Q., King, S. M., Rosenoern, T., Kroll, J. H., Worsnop, D. R., McKinney, K. A., and Martin, S. T.: Particle mass yield in secondary organic aerosol formed by the dark ozonolysis of α-pinene, Atmos. Chem. Phys., 8, 2073–2088, doi:10.5194/acp-8-2073-2008, 2008.

Shrivastava, M., Fast, J., Easter, R., Gustafson Jr., W. I., Zaveri, R. A., Jimenez, J. L., Saide, P., and Hodzic, A.: Modeling organic aerosols in a megacity: comparison of simple and complex representations of the volatility basis set approach, Atmos. Chem. Phys., 11, 6639–6662, doi:10.5194/acp-11-6639-2011, 2011.

Shrivastava, M. K., Lane, T. E., Donahue, N. M., Pandis, S. N., and Robinson, A. L.: Effects of gas particle partitioning and aging of primary emissions on urban and regional organic aerosol concentrations, J. Geophys. Res.-Atmos., 113, D18301, doi:10.1029/2007jd009735, 2008.

Song, C., Na, K. S., and Cocker, D. R.: Impact of the hydrocarbon to NO_x ratio on secondary organic aerosol formation, Environ. Sci. Technol., 39, 3143–3149, doi:10.1021/es0493244, 2005.

ACPD
13, 15907–15947, 2013

Song, C., Na, K., Warren, B., Malloy, Q., and Cocker, D. R.: Secondary organic aerosol formation from the photooxidation of *p*- and *o*-xylene, Environ. Sci. Technol., 41, 7403–7408, doi:10.1021/es0621041, 2007.

Spracklen, D. V., Jimenez, J. L., Carslaw, K. S., Worsnop, D. R., Evans, M. J., Mann, G. W., Zhang, Q., Canagaratna, M. R., Allan, J., Coe, H., McFiggans, G., Rap, A., and Forster, P.: Aerosol mass spectrometer constraint on the global secondary organic aerosol budget, Atmos. Chem. Phys., 11, 12109–12136, doi:10.5194/acp-11-12109-2011, 2011.

Strader, R., Lurmann, F., and Pandis, S. N.: Evaluation of secondary organic aerosol formation in winter, Atmos. Environ., 33, 4849–4863, doi:10.1016/s1352-2310(99)00310-6, 1999.

Surratt, J. D., Chan, A. W. H., Eddingsaas, N. C., Chan, M. N., Loza, C. L., Kwan, A. J., Hersey, S. P., Flagan, R. C., Wennberg, P. O., and Seinfeld, J. H.: Reactive intermediates revealed in secondary organic aerosol formation from isoprene, P. Natl. Acad. Sci. USA, 107, 6640–6645, doi:10.1073/pnas.0911114107, 2010.

Takekawa, H., Minoura, H., and Yamazaki, S.: Temperature dependence of secondary organic aerosol formation by photo-oxidation of hydrocarbons, Atmos. Environ., 37, 3413–3424, doi:10.1016/s1352-2310(03)00359-5, 2003.

Tsimpidi, A. P., Karydis, V. A., Zavala, M., Lei, W., Molina, L., Ulbrich, I. M., Jimenez, J. L., and Pandis, S. N.: Evaluation of the volatility basis-set approach for the simulation of organic aerosol formation in the Mexico City metropolitan area, Atmos. Chem. Phys., 10, 525–546, doi:10.5194/acp-10-525-2010, 2010.

Tsimpidi, A. P., Karydis, V. A., Zavala, M., Lei, W., Bei, N., Molina, L., and Pandis, S. N.: Sources and production of organic aerosol in Mexico City: insights from the combination of a chemical transport model (PMCAMx-2008) and measurements during MILAGRO, Atmos. Chem. Phys., 11, 5153–5168, doi:10.5194/acp-11-5153-2011, 2011.

Updyke, K. M., Nguyen, T. B., and Nizkorodov, S. A.: Formation of brown carbon via reactions of ammonia with secondary organic aerosols from biogenic and anthropogenic precursors, Atmos. Environ., 63, 22–31, doi:10.1016/j.atmosenv.2012.09.012, 2012.

Wang, S. C., Paulson, S. E., Grosjean, D., Flagan, R. C., and Seinfeld, J. H.: Aerosol formation and growth in atmospheric organic nox systems, 1. Outdoor smog chamber studies of C-7-hydrocarbons and C-8-hydrocarbons, Atmos. Environ. A, 26, 403–420, doi:10.1016/0960-1686(92)90326-g, 1992.

Xie, Y., Paulot, F., Carter, W. P. L., Nolte, C. G., Luecken, D. J., Hutzell, W. T., Wennberg, P. O., Cohen, R. C., and Pinder, R. W.: Understanding the impact of recent advances in iso-

ACPD
13, 15907–15947, 2013

prene photooxidation on simulations of regional air quality, Atmos. Chem. Phys. Discuss., 12, 27173–27218, doi:10.5194/acpd-12-27173-2012, 2012.

Yu, J. Z., Cocker, D. R., Griffin, R. J., Flagan, R. C., and Seinfeld, J. H.: Gas-phase ozone oxidation of monoterpenes: gaseous and particulate products, J. Atmos. Chem., 34, 207–258, 1999.

Zhang, H. L. and Ying, Q.: Secondary organic aerosol from polycyclic aromatic hydrocarbons in Southeast Texas, Atmos. Environ., 55, 279–287, doi:10.1016/j.atmosenv.2012.03.043, 2012.

Zhou, Y., Zhang, H. F., Parikh, H. M., Chen, E. H., Rattanavaraha, W., Rosen, E. P., Wang, W. X., and Kamens, R. M.: Secondary organic aerosol formation from xylenes and mixtures of toluene and xylenes in an atmospheric urban hydrocarbon mixture: Water and particle seed effects (II), Atmos. Environ., 45, 3882–3890, doi:10.1016/j.atmosenv.2010.12.048, 2011.

ACPD
13, 15907–15947, 2013

Table 1. 2p-VBS parameters, based on VBS parameters of Tsimpidi et al. (2010), for SOA precursors under high- and low-NOx conditions at $T = 298\,\mathrm{K}$ and $\rho = 1.5\,\mathrm{g\,cm^{-3}}$.

	High NO_x					Low NO_x				
Precursor	α_1	C_1^*	α_2	C_2^*	Data Sources	α_1	C_1^*	α_2	C_2^*	Data Sources
ALK4	0.038	10				0.075	10			
ALK5	0.150	10			a, b,c	0.300	10			
OLE1	0.009	9.0	0.116	284		0.014	4.0	0.170	236	
OLE2	0.032	8.1	0.216	244		0.055	2.8	0.297	170	
ARO1 = TOL	0.186	10	0.488	180		0.218	3.2	0.625	103	d, e
ARO2 = XYL	0.219	11	0.487	185	d	0.275	3.7	0.639	97	
ISO	0.020	7.4	0.018	68	f	0.019	2.1	0.032	28	
TERP	0.130	7.3	0.433	191		0.160	1.7	0.615	126	
SESQ (fit for $M_o \leq 30\,\mu\mathrm{g\,m^{-3}}$)	0.647	18			g, h,i	n/a				

Data sources for the Tsimpidi et al. (2010) parameterizations are provided if specifically discussed in the text.
[a] Wang et al. (1992).
[b] Takekawa et al. (2003).
[c] Lim and Ziemann (2005).
[d] Ng et al. (2007b).
[e] Hildebrandt et al. (2009).
[f] Pandis et al. (1991).
[g] Hoffmann et al. (1997).
[h] Griffin et al. (1999).
[i] Ng et al. (2007a).

ACPD
13, 15907–15947, 2013

Table 2. 2p-VBS parameters based on VBS parameters for alkanes (Presto et al., 2010), naphthalene (Pye et al., 2010), undefined POA (Shrivastava et al., 2008), wood smoke POA and diesel POA (Grieshop et al., 2009) under high-NOx conditions for $T = 298\,\mathrm{K}$ and $\rho = 1.0\,\mathrm{g\,cm^{-3}}$.

Precursor	α_1	C_1^*	$\Delta H_{vap,1}$	α_2	C_2^*	$\Delta H_{vap,2}$
$C_{12}H_{26}$	0.091	4.7	30	0.569	218	30
$C_{13}H_{28}$	0.121	1.1	30	0.666	52.6	30
$C_{14}H_{30}$	0.139	0.7	30	0.675	31.4	30
$C_{15}H_{32}$	0.155	0.6	30	0.674	23.4	30
$C_{16}H_{34}$	0.167	0.5	30	0.672	19.0	30
$C_{17}H_{36}$	0.183	0.5	30	0.664	16.0	30
Naphthalene	0.144	2.9	30	0.226	33.7	30
POA	0.257	0.7	112	0.501	180	77
Wood Smoke POA	0.228	1.6	69	0.473	103	56
Diesel POA	0.239	4.4	66	0.479	213	58

ACPD
13, 15907–15947, 2013

Table 3. Default parameters (base case) and best available parameters for biogenic high-NOx (BA-highNOx) and biogenic low-NOx (BA-lowNOx) CMAQv4.7.1 simulations[a]; T = 298 K and densities[b] matched to reported densities for base case (Carlton et al., 2010).

	Base Case				Best Available (BA)				
Precursor	α_1	C_1^*	α_2	C_2^*	α_1	C_1^*	α_2	C_2^*	Source
ALK5	0.072	0.02			0.10	6.7			2p-VBS
TOL = ARO1[c]	0.076	2.3	0.148	21.3	0.201	8.5	0.527	149	2p-VBS
XYL = ARO2[c]	0.039	1.3	0.112	34.5	0.039	1.3	0.112	34.5	CMAQ
ISO	0.029	0.6	0.232	116	0.029	0.6	0.232	116	CMAQ
TERP (high-NOx)	0.139	14.8	0.454	134	0.112	6.3	0.376	165	2p-VBS
TERP (low-NOx)	n/a				0.139	1.5	0.533	110	2p-VBS
SQT = SESQ	1.537	25.0			1.537	25.0			CMAQ

[a] NO_x dependent SOA pathways for anthropogenic compounds are treated in CMAQv.4.7.1, with branching calculated as a function of RO_2 reaction with NO vs. HO_2. Only the high-NOx anthropogenic parameters are shown here; the CMAQ default low-NOx anthropogenic parameters were used in all simulations. High-NOx and low-NOx biogenic cases were run to illustrate the limits of SOA production in each of these scenarios (note: only the TERP parameters vary with NO_x level, see text for discussion).

[b] Density, ρ ($g\,cm^{-3}$): ALK5, 1.0; TOL, 1.24; XYL, 1.48; ISO, 1.4; TERP, 1.3; SQT, 1.3.

[c] Each α value (CMAQ and 2p-VBS) was divided by 0.765 (TOL) or 0.804 (XYL) to account for a stoichiometric factor in the implementation of the SAPRC mechanism in CMAQv4.7.1.

ACPD
13, 15907–15947, 2013

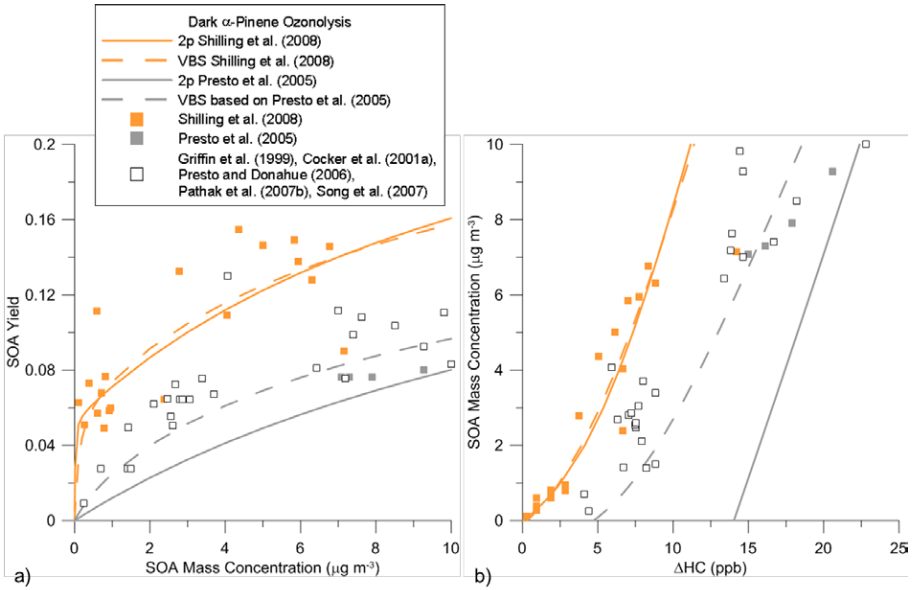

Fig. 1. Comparison of 2p (solid lines) and VBS (dashed lines) parameterizations for dark α-pinene ozonolysis chamber experiments, as influenced by the range in SOA mass concentration and number of data points at low SOA mass loading. Panel **(a)** SOA yield vs. SOA mass concentration; panel **(b)** SOA mass concentration vs. level of reacted hydrocarbon (ΔHC).

ACPD
13, 15907–15947, 2013

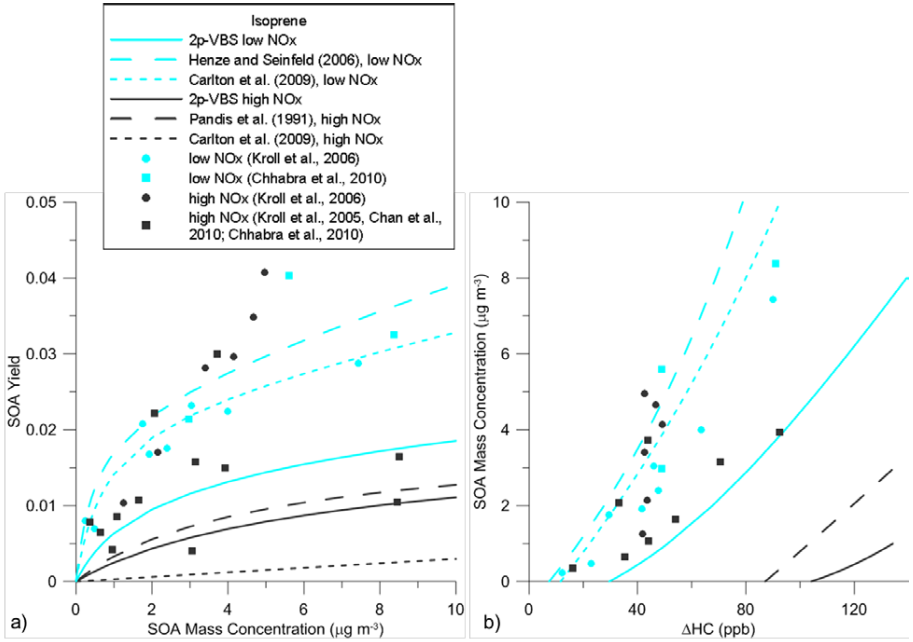

Fig. 2. Evaluation of 2p and 2p-VBS parameterizations for isoprene under low-NOx (cyan) and high-NOx (black) conditions. Panel **(a)** theoretical yield curve (SOA yield vs. SOA mass concentration); panel **(b)** predicted SOA mass curve (SOA mass concentration vs. level of reacted hydrocarbon, ΔHC).

ACPD
13, 15907–15947, 2013

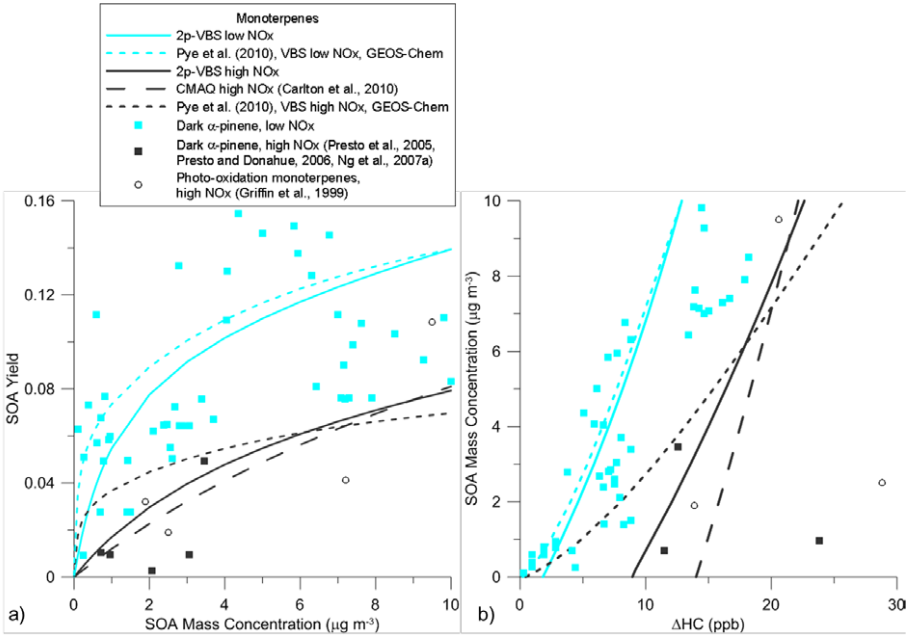

Fig. 3. Evaluation of 2p and 2p-VBS parameterizations for lumped monoterpenes under low-NOx (cyan) and high-NOx (black) conditions. Panel **(a)** theoretical yield curve (SOA yield vs. SOA mass concentration); panel **(b)** predicted SOA mass curve (SOA mass concentration vs. level of reacted hydrocarbon, ΔHC).

ACPD
13, 15907–15947, 2013

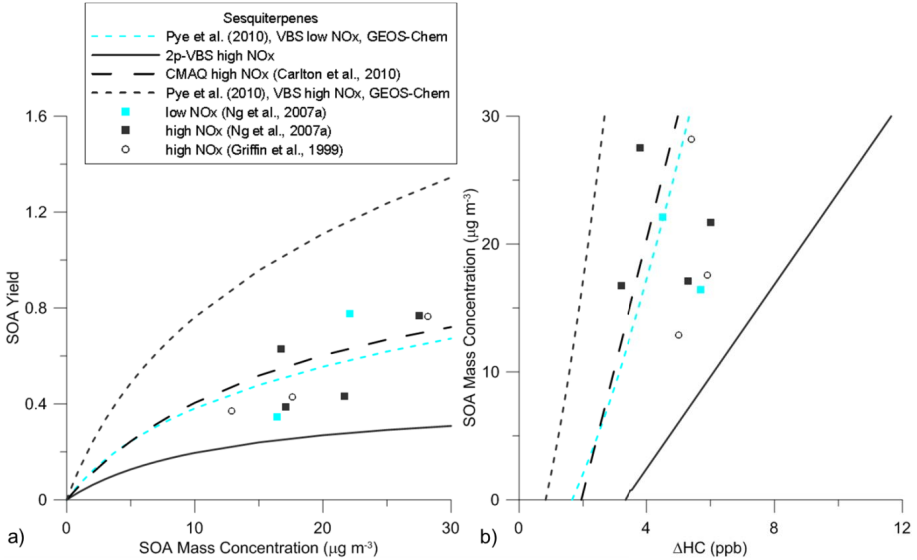

Fig. 4. Evaluation of 2p and 2p-VBS parameterizations for lumped sesquiterpenes under low-NOx (cyan) and high-NOx (black) conditions. Panel **(a)** theoretical yield curve (SOA yield vs. SOA mass concentration); panel **(b)** predicted SOA mass curve (SOA mass concentration vs. level of reacted hydrocarbon, ΔHC).

ACPD
13, 15907–15947, 2013

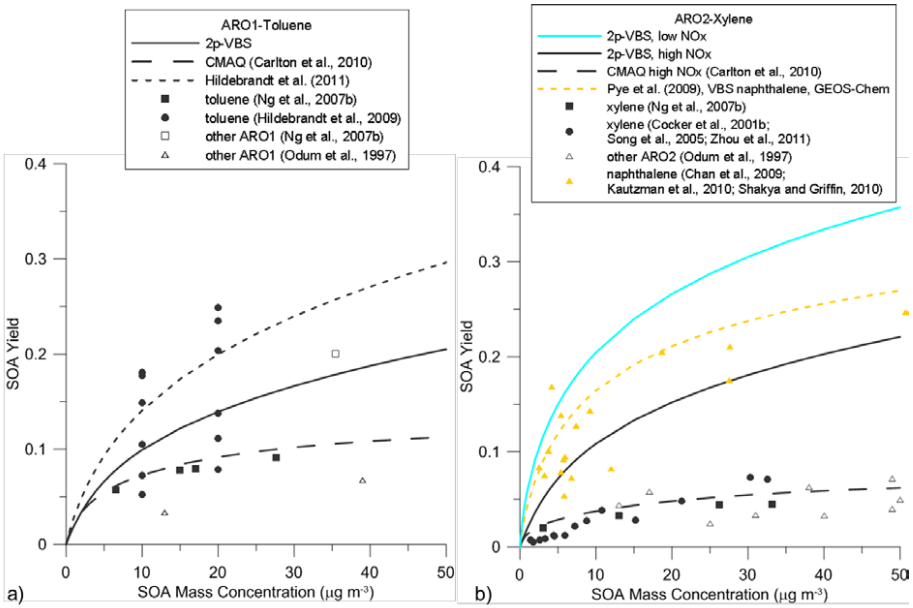

Fig. 5. Evaluation of 2p and 2p-VBS parameterizations for lumped aromatics. Panel **(a)** ARO1/toluene theoretical yield curve (SOA yield vs. SOA mass concentration); panel **(b)** ARO2/xylene theoretical yield curve.

ACPD
13, 15907–15947, 2013

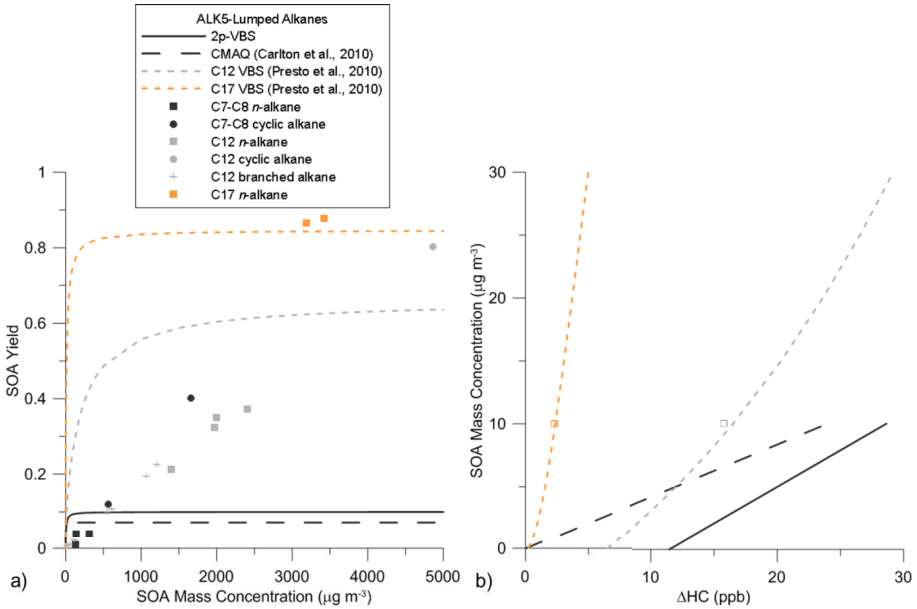

Fig. 6. Evaluation of 2p and 2p-VBS parameterizations for lumped alkanes (≥ C6). Panel **(a)** theoretical yield curve (SOA yield vs. SOA mass concentration); panel **(b)** predicted SOA mass curve (SOA mass concentration vs. level of reacted hydrocarbon, ΔHC) for $M_o \leq 30\,\mu g\,m^{-3}$. Filled symbols data from Lim and Ziemann (2009); open symbols data from Presto et al. (2010).

ACPD
13, 15907–15947, 2013

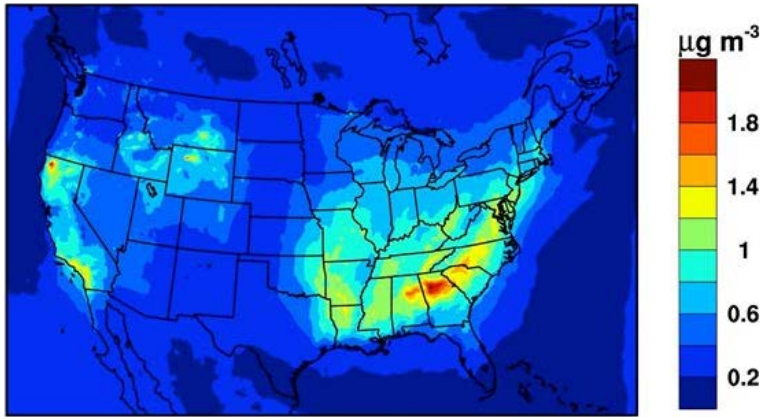

Fig. 7. Total SOA averaged over 15–31 July 2006 for the base case simulation (using default CMAQ parameters).

ACPD
13, 15907–15947, 2013

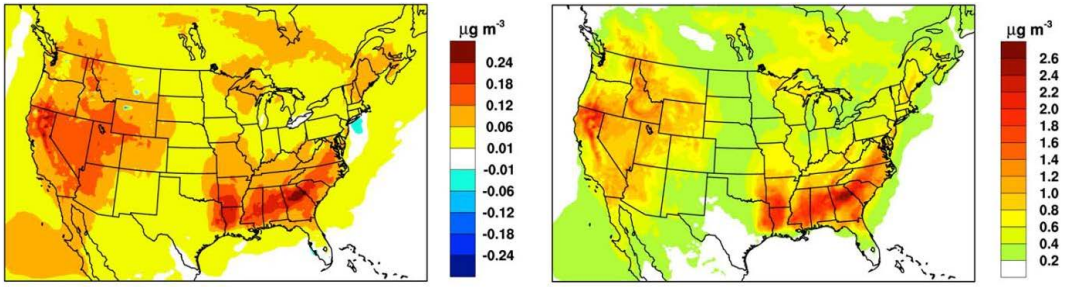

a) Best available w/high NOx 2p-VBS terpenes

b) Best available w/low NOx 2p-VBS terpenes

Fig. 8. Difference in total SOA averaged over 15–31 July 2006 between the best available parameter simulation and the base case CMAQ simulation: using the high-NOx 2p-VBS parameters for lumped monoterpenes (panel **a**), and using the low NOx 2p-VBS parameters for lumped monoterpenes (panel **b**).

ACPD
13, 15907–15947, 2013

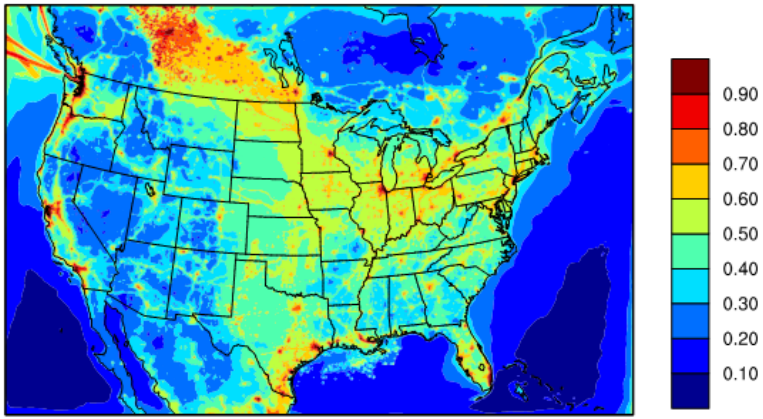

Fig. 9. The fraction of RO_2 reacting with NO (vs. HO_2), indicating the relative importance of high- vs. low-NOx pathways, respectively, predicted in the CMAQ simulations averaged over the simulation period, 15–31 July 2006.

ACPD
13, 15907–15947, 2013